The International Journal of Advanced Manufacturing Technology (2023) 128:257–266
https://doi.org/10.1007/s00170-023-11701-w

ORIGINAL ARTICLE

Formation of highly ordered TiO_2 nanotubes on Ti6Al4V alloys manufactured by electron beam powder bed fusion (E-PBF)

Robinson Aguirre Ocampo[1] · Nicolás Bedoya Ochoa[2] · José A. Tamayo[3] · Carlos Botero[4] · Carlos Andrés Vargas[3] · Maryory Gómez[1] · Juan Guillermo Castaño[1] · Alejandro A. Zuleta Gil[5]

Received: 9 February 2023 / Accepted: 31 May 2023 / Published online: 6 July 2023

Abstract
Highly ordered TiO_2 nanotubes were obtained by anodization on Ti6Al4V substrates manufactured by electron beam powder bed fusion (E-PBF). Effects of anodization parameters such as anodizing time, stirring, fluoride concentration, and water content were analyzed in an organic electrolyte (ethylene glycol) that contains ammonium fluoride. The ordering of the nanotubes was measured by regularity ratio calculations based on fast Fourier transform (FFT) from SEM images. It was found that for the processed specimens, the highest ordering of the TiO_2 nanotubes was reached at 30 V for 5000 s with a concentration of 9 vol% H_2O and 0.4 wt.% NH_4F, exhibiting nanotubes free of delamination, cracks, and coral-like structures with a regularity ratio (RR) of 1.91. This work offers a simple method for creating homogeneous and organized TiO_2 nanotubes on Ti6Al4V substrates manufactured by E-PBF which potentially improves its functionality in diverse industrial applications such as nanosensors, controlled-release substances, solar cells, water splitting, electrochromic devices, and Li-ion battery anodes.

Keywords Additive manufacturing · Anodizing · Electron beam melting · TiO_2 nanotubes · Self-organized nanotubes

1 Introduction

Titanium and its alloys have excellent properties such as good corrosion behavior, low density, high stiffness to weight ratio, strength, and fracture toughness [1], which makes them attractive for a wide range of applications in fields such as aerospace, biomedical, chemical and automotive, petrochemical, and pharmaceutical [2, 3]. Particularly, Ti6Al4V is the most prevalent and extensively used titanium alloy, supplying nearly half of the global market of titanium-based products [4, 5]. It is expected that the titanium global market to reach US$ 6.24 billion by 2027 [5, 6] mainly driven by the increasing demand for biomedical devices and manufacturing of lighter components for transport and the launch of technologically advanced products.

Components made of titanium and its alloys have conventionally been manufactured by casting, forging, extrusion, and powder metallurgy manufacturing methods. These methods include several processing stages due to the high reactivity of titanium. Some of those processes allow for the formation of alpha case layer affecting the mechanical properties of the part [7], which is critical at melting temperatures and during thermal processing [7]. In addition, Ti6Al4V alloys, compared to other materials, are difficult to machine and weld, which causes processing costs to increase, especially when dealing with complex morphologies [4]. The above implies that the manufacturing of parts of titanium alloys requires the adoption of technologies with precise control of the processing parameters and variables

✉ Robinson Aguirre Ocampo
robinson.aguirre@udea.edu.co

1 Centro de Investigación, Innovación y Desarrollo de Materiales – CIDEMAT, Facultad de Ingeniería, Universidad de Antioquia UdeA, Calle 70 No 52 – 21, Medellín, Colombia

2 Programa de Ingeniería en Nanotecnología, Universidad Pontificia Bolivariana, Sede Medellín, Circular 1 No 70-01, Medellín, Colombia

3 Grupo Calidad Metrología Y Producción, Instituto Tecnológico Metropolitano –ITM-, 050034 Medellín, Antioquia, Colombia

4 Sports Tech Research Centre, Department of Quality Management and Mechanical Engineering, Mid Sweden University, Akademigatan 1, 83125 Östersund, Sweden

5 Grupo de Investigación de Estudios en Diseño - GED, Facultad de Diseño Industrial, Universidad Pontificia Bolivariana, Sede Medellín, Circular 1 No 70-01, Medellín, Colombia

to avoid contamination of the material by external elements, which are difficult to extract by subsequent processes. In this sense, and thanks to the accelerated use of titanium, many industrial sectors have taken advantage of techniques such additive manufacturing (AM) since they allow shortening delivery and lead times, reducing costs, solving difficulties, and geometrical restrictions, but also making it possible the production of lighter objects and with less environmental impact since the use of material is optimized during the manufacturing [7, 8] what ultimately brings a shortened product development cycle [8]. In addition, AM is useful for obtaining components used in electrochemistry and for photovoltaic cells, electrodes, and photoelectrodes with particular morphologies [9] that simultaneously increase the surface area from the formation, for example, of cellular structures, enhancing its potential applications. According with the ASTM F2792-12a, there are three main categories that have been used for processing titanium and its alloys [10]: (i) directed energy deposition (DED), (ii) Ultrasonic additive manufacturing (UAM), and (iii) powder bed fusion (PBF), the latter standing for more than 80% of the global metal AM market. In PBF, powder particles spread in a bed are selectively fused or melted, layer by layer, by the action of either a laser (L-PBF) or an electron beam (E-PBF), to build parts of a desired 3D geometry [8, 11–13]. One of the main technologies within E-PBF is electron beam melting, also referred as electron beam powder bed fusion (E-PBF). In E-PBF, the parts are built in a vacuum environment at high temperatures (600–700 °C in the case of Ti alloys), allowing for manufacturing of high-quality components with complex geometries. E-PBF has therefore been extensively used for manufacturing of Ti6Al4V in biomedical applications [11, 14]. In addition, E-PBF components have enhanced ductility in contrast with forged specimens [10, 15]. Additionally, since a powerful electron beam is steered by electromagnetic lenses in E-PBF, the parts can be produced with a faster build rate in contrast with L-PBF and other metal AM techniques such as DED, due its faster scan rate and superior energy input [16].

Despite the demonstrated benefits of the manufacturing of Ti6Al4V alloys by E-PBF and the great interest from several industrial fields [16], there are still aspects regarding the surface of the materials obtained, as well as its improvement or functionalization, that continue to be poorly studied. This is especially relevant in applications such as biomedical, where the role of the surface is critical in the function and performance of components. Anodizing is one of the most interesting surface modification processes due to its good reproducibility, simplicity, low-cost, and the fact that no complex equipment is needed [17, 18]. Furthermore, a special interest in anodization has been given to the formation of 1D-nanostructures such a TiO_2 nanotubes (TNT) [19–23], which has been proposed as a promising application in many industrial fields ranging from water treatment with photovoltaic systems to biomedical applications, including nanosensors [24], controlled-release substances [25], solar cells [26], water splitting [27], electrochromic devices [28], Li-ion battery anodes [24], osteointegration promoters, and antibacterial agents reservoirs for prosthetic implants [17, 22, 29, 30]. In addition to the advantages mentioned above, the anodizing technique offers the possibility of producing coatings on parts with rather complex geometries. This makes it a suitable technique to apply surface modifications in parts manufactured by AM processes like E-PBF, where often personalized parts with complex shapes are manufactured. It would be then virtually possible to obtain 1D-nanostructures basically on any type of Ti6Al4V pieces printed by E-PBF. One of the aspects that deserves further research in relation to the TNT formation is the control of its morphology and distribution on the surface. The organization of the nanotubes allows better control of the properties making them a promising functional material for various applications. It is important to mention that most of the published reports about TNT formation, especially for organic electrolytes, are in regard to commercially pure titanium substrates and not much information is available on TNT formed on ternary Ti alloys [29]; however, many applications require the use of substrates with better mechanical performance such as Ti6Al4V titanium alloys. According with the reported by Macak and collaborators [31] experienced difficulties in their attempts to form highly organized TNT on Ti6Al4V substrates, specially due to the dissolution and different reaction rates of the phases in the alloys, which in the case of the E-PBF process is a matter that has not been addressed given the particularity of the process and the distribution characteristics of the alpha and beta phases in the coating [1, 4, 29]. To the best of our knowledge, reports about the formation of anodic layers on Ti6Al4V manufactured by E-PBF is scarce, especially regarding the formation of highly organized TiO_2 nanotubes on this type of substrates.

The aim of this study is therefore to obtain highly organized TiO_2 nanotubes on Ti6Al4V substrates manufactured by AM using a single-step anodization process. In doing so, disc shaped samples fabricated by E-PBF were anodized using a two-electrode configuration in ethylene glycol solution containing water (2–10 vol.%), aiming to generate 1D-nanostructures under potentiostatic conditions at a potential of 30 and 60 V as well as to determine the influence of the potential and composition on the morphology and organization of the nanotubes. The novelty of this work is related to the demonstration of an experimental methodology that allows obtaining highly ordered TiO_2 nanotubes on Ti6Al4V substrates manufactured by E-PBF analyzed by regularity measurement ratio calculations based on FFT images. This type of analysis does not show before for this kind of 3D-manufactured substrate. To date, this type of

analysis has not been reported in this way for Ti6Al4V substrates fabricated by additive manufacturing.

2 Experimental

2.1 Substrate preparation

Ti6Al4V substrates were manufactured using the electron beam powder bed fusion (EB-PBF) technology using an Arcam A2 electron beam melting (EBM) system (ARCAM, Mölndal, Västra Götaland, Sweden). Substrates were built at an acceleration voltage of 60 kV (producing a beam with a maximum power of 4 kW), in a vacuum environment (~ 10^{-4} mbar), an operating temperature of 600–700 °C and a layer thickness of 50 um. The microstructure of the substrates was analyzed by SEM after the metallographic preparation, which was performed by polishing the specimens using SiC abrasive paper up to mirror finish and then etched in a Kroll's reagent and ultrasonically cleaned in acetone and distilled water. The composition of the obtained substrate was determined by optical emission spectroscopy (using a Q4 TASMAN equipment) is summarized in Table 1. Then, coupons of 19 mm and 3 mm in diameter and thick, respectively, were cut from the printed specimen and ground with SiC abrasive paper of different grit sizes until #1200. They were then cleaned with ethanol using an ultrasonic probe and finally drying in air.

2.2 Anodization process

The anodizing process was carried out under potentiostatic conditions using an ethylene glycol-based bath. The samples denomination and process conditions are given in Table 2. The anodizing solutions were prepared under stirring at 400 RPM for 1 h. In all cases, the Ti6Al4V substrates obtained by electron beam powder bed fusion were used as anode and a graphite plate as cathode. After the anodization process, the specimens were rinsed with distilled water and then immersed in a beaker with ethylene glycol to avoid further dissolution of the formed anodic film. Finally, the samples were rinsed with distilled water and finally dried in air. For each condition, each experiment was repeated three times.

2.3 Anodic layer characterization

The chemical composition and structure of the anodic layers was studied by Raman spectroscopy by using a Labram High Resolution Jovin Yvon Horiba equipment. Surface analysis and morphology characterization were carried out using a ThermoFisher Scientific Apreo 2 field emission scanning electron (FESEM) microscopy equipped with ThermoFhisher energy-dispersive X-ray (EDX) microprobe. Cross-sections of coatings were prepared by scratching the sample with a scalpel and then tilting the SEM holder until getting the desired image. To measure the nanotubes organization, a quantitative fast Fourier transformation (FFT) analysis was made by using SEM images of the specimen's surfaces. The FFT analysis were made using the WSxM 5.0 software [32] and other measurements as internal diameter and coating thickness were made using the xT Microscope Version 23.2.0 of Thermo Fisher Scientific software and a public domain software Image J®.

3 Results and discussion

SEM cross-sectional micrographs of Ti6Al4V substrates manufactured by E-PBF in a cut perpendicular to the build direction are presented in Fig. 1. The microstructure consists of β platelets (of between 0.5 and 2.5 μm in length) and retained particles uniformly distributed in a fine-lath alpha phase matrix. This configures both a colony- and basket-weave morphology within prior beta grains (also referred to

Table 1 Chemical composition (wt. %) of the E-PBF processed substrates

Element	Si	Al	Mo	Nb	V	Zr	Fe	Co	Cu	Cr	Ti
%	0.041	6.030	0.013	0.069	4.371	< 0.010	0.128	0.013	0.0024	0.0059	Bal

Table 2 Bath composition and process conditions

Sample ID	Solution composition	Voltage (V)	Time (sec)	Stirring
M1	9 vol% H_2O, 0.4 wt.% NH_4F	30	5000	No
M2	9 vol% H_2O, 0.4 wt.% NH_4F	30	5000	Yes
M3	9 vol% H_2O, 0.4 wt.% NH_4F	60	5000	No
M4	4.5 vol% H_2O, 0.4 wt.% NH_4F	30	5000	No
M5	9% vol% H_2O, 0.4 wt.% NH_4F	30	1000	No
M6	9% vol% H_2O, 0.4 wt.% NH_4F	30	2500	No
M7	9% vol% H_2O, 0.2 wt.% NH_4F	30	5000	No

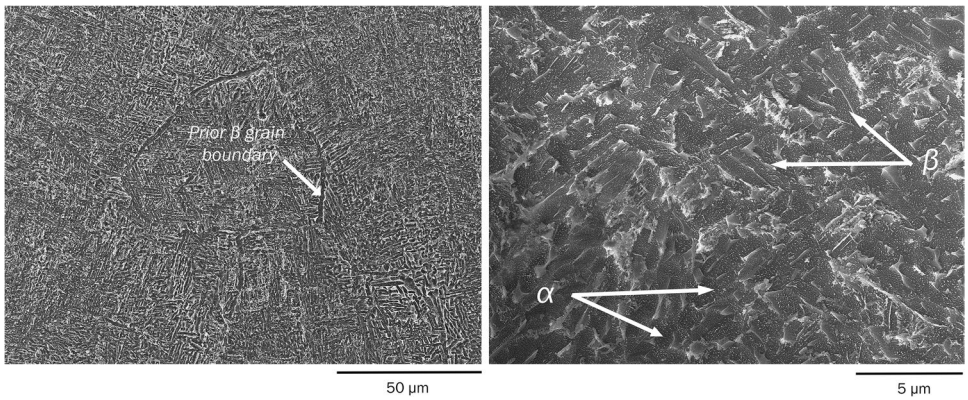

Fig. 1 As-built microstructures of the Ti6Al4V substrates manufactured by E-PBF

as Widmastätten microstructure). Similar microstructures have been reported in the literature [33–35] for these type of substrates.

The presence of both α and β phases has a relevant effect on the growth of the anodic layer since there are different electrochemical behavior as consequence of the microstructure and the compositional differences of the α and β phases which can undergo different anodizing rates [4]. It has been demonstrated the presence of bimodal α/β phases significantly affects the regularity and homogeneity of the formed TiO_2 nanotubes [36]. In addition, it has reported that apparently the formation of highly organized TNT over a large surface area can be obtained only on single phase titanium alloys like cp-Ti sheets but more difficult on binary or ternary alloys such as Ti6Al4V [29, 37]. However, controversially to this and according with the results that will be shown below, the formation of self-organized and regular TNT on the whole of treated area is possible on E-PBF substrates. Regarding this, Fig. 2 shows low magnification images of the treated surface exhibiting, a well distributed and regular formation of TNT on it with the presence of apparent cavities whose shape, length, and distribution are corresponding with β platelets observed in Fig. 1, is then evident, as mentioned above, a lower growth kinetics for nanotubes in such phases. From Fig. 2, it worth to highlight that the nanotube structures obtained in this experimental work are free of delamination, cracks, and coral-like structures. This type of defects have been reported in a recent paper [38] in which they produced TiO_2 nanotubes over a Ti6Al4V substrate obtained by SLM.

A curve of current density vs. time during the anodization of Ti6Al4V substrates manufactured by E-PBF in ethylene glycol is shown in Fig. 3. The shape of the curve has the characteristic form associated with the TiO_2 nanotube formation [23, 29, 39]; furthermore, the curve shape in the Fig. 3 is similar to the curve form obtained in Ti6Al4V substrates manufactured by forging [38].

Three stages in the nanotube's formation are seen in Fig. 3. The first stage is related to the formation of a barrier layer; in this stage, the current density surges suddenly before falling quickly [39]. Before reaching a minimum value, stage 2 starts; in this stage, by limiting the flow of oxygen molecules through the barrier layer, the oxide thickness obtained at this point causes the balance between oxidation and dissolution to tip in favor of dissolution and increases pore formation [40]. This process persists until the maximum pore density is achieved when the current density achieves a maximum. Next, the current density diminishes, and the nanopores rearrange and contend with one another to develop into nanotubes [39]. Stage 3 initiates at the point where the slant of the curve change; in this step, the pores have been converted into nanotubes, and as time progresses, the nanotubes grow in length [41].

To obtain highly ordered and clean (nanotubes free of particles or incompletely dissolved oxide layers on their top) TiO_2 nanotubes on Ti6Al4V alloys manufactured by E-PBF, we studied experimental anodization conditions, such as anodizing time, stirring, fluoride concentration, and water content. Regarding the electrolyte stirring effect on the TiO_2 nanotube morphology and organization, we compared the nanotube obtained from M1 and M2 samples (see Table 2).

Figure 2 shows low and high magnification SEM images of the TiO_2 nanotubes obtained at the different anodizing conditions listed in Table 2. From Table 2, the only difference between the M1 and M2 samples is the electrolyte stirring; the M2 sample is stirring. From Fig. 2, nanotubes were formed in both samples; however, the nanotube of the M2 sample has particles on its top in contrast to the nanotubes produced in the M1 sample. These undesirable particles could be related to the electrolyte stirring; according to several authors [42–47], electrolyte stirring directly affects the nanotube morphology and could produce damage in the nanotube top, which is the cause of the presence of these particles [42, 46]. However, these unwanted particles could be eliminated using ultrasonic agitation; but this extra step might damage the nanotube structure [48]. Figure 4 shows the SEM images of the cross-section view of TiO_2 nanotubes obtained on Ti6Al4V substrates manufactured by E-PBF.

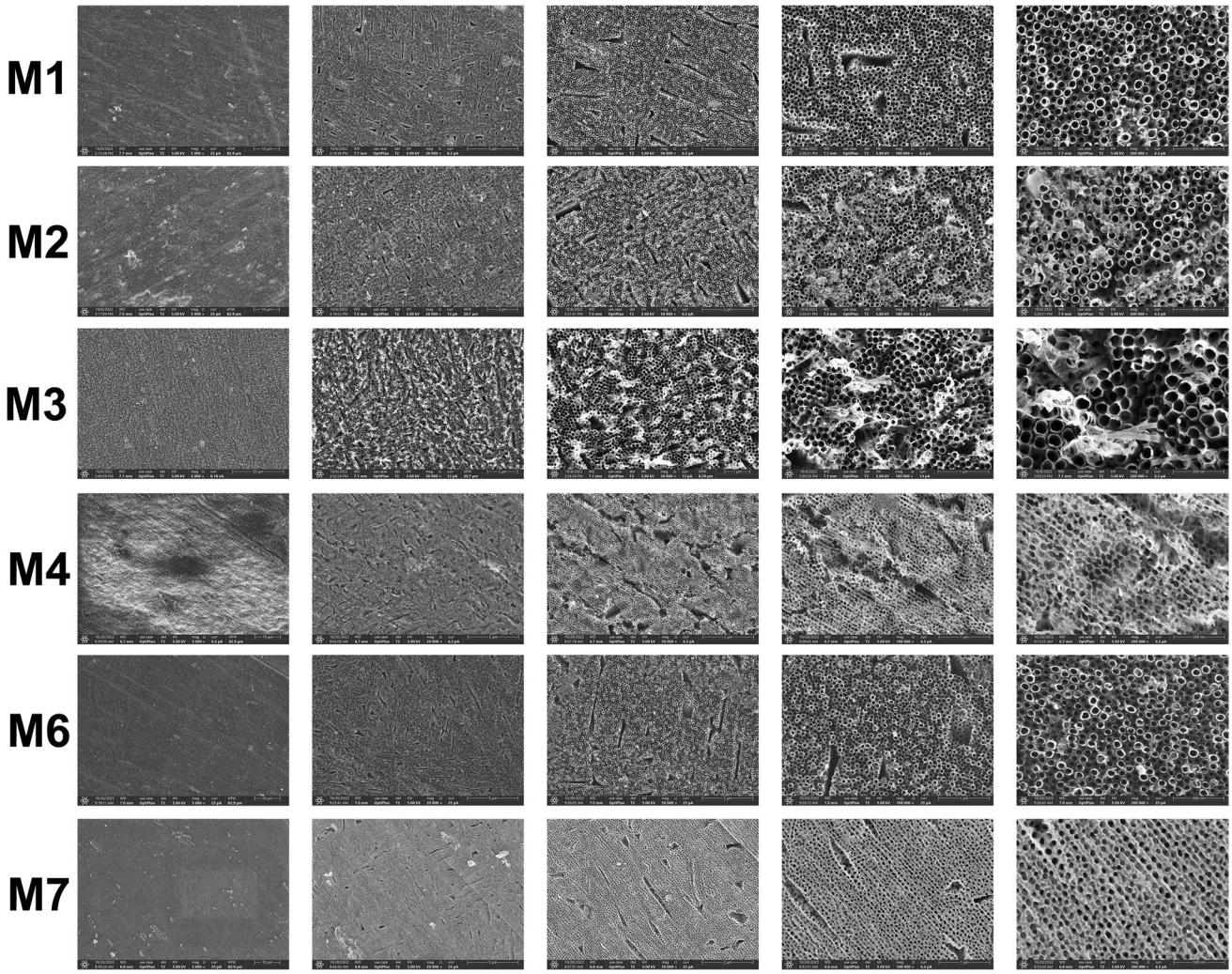

Fig. 2 SEM images from low (left) to high (right) magnifications of TiO_2 nanotubes obtained on Ti6Al4V substrates manufactured by E-PBF

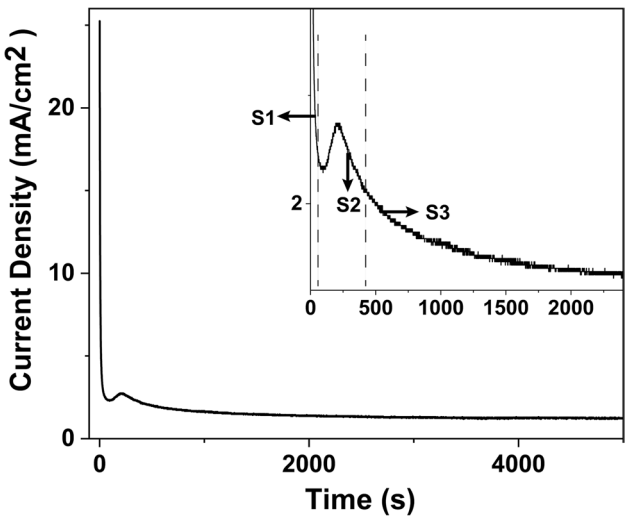

Fig. 3 Current vs. time responses during the anodization of Ti6Al4V substrates manufactured by E-PBF

Table 3 lists the internal diameter, length, and circularity values of TiO_2 nanotubes obtained on Ti6Al4V substrates manufactured by E-PBF. From Fig. 4 and Table 3, the electrolyte stirring does not affect internal diameter.

On the other hand, there is a slight difference in nanotube length between the samples M1 and M2. According to the scientific literature [44, 47], the nanotubes produced in stirred electrolytes have a longer length in contrast to the nanotubes produced in non-stirred electrolytes. Our findings conflict with the conclusions of these investigations.

Anodization time is an important parameter to obtain highly ordered nanotubes; it necessarily chooses an anodizing time that allows higher self-organization. Thus, we evaluated three anodization times to obtain the lowest anodization time that permits achieving highly ordered nanotubes. From Table 2, M5, M6, and M1 samples have anodization times of 1000, 2500, and 5000 s, respectively. From Fig. 4, nanotubes were formed in the M5 sample; however, those

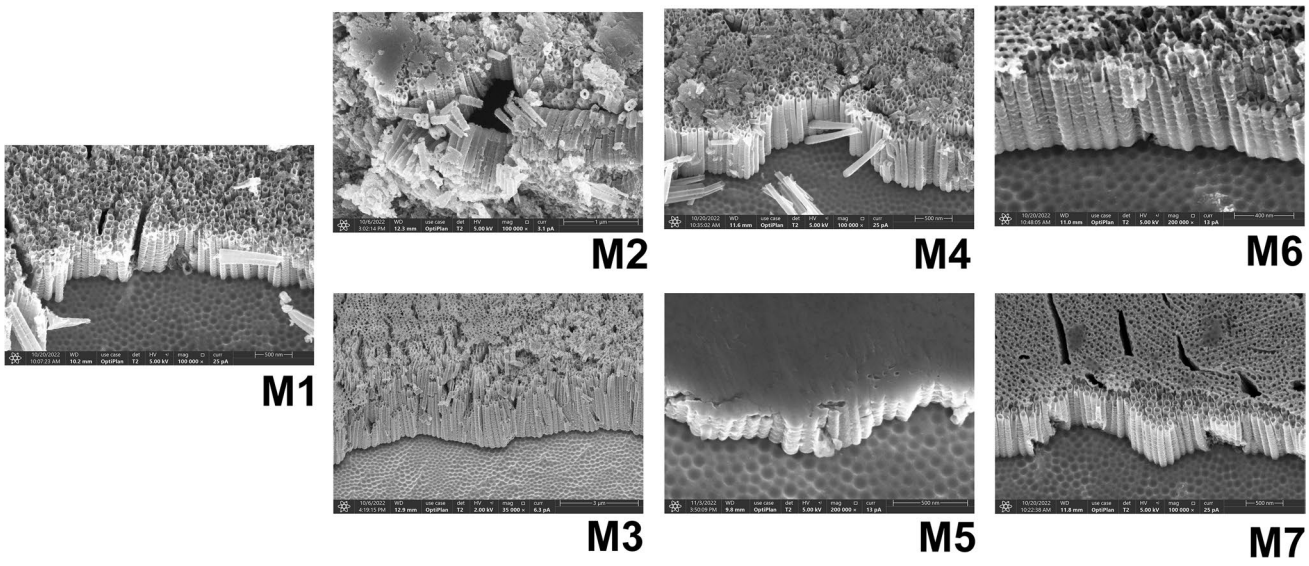

Fig. 4 SEM images of the cross-section view of TiO_2 nanotubes obtained on Ti6Al4V substrates manufactured by E-PBF

Table 3 Internal diameter, length, and circularity of TiO_2 nanotubes obtained on Ti6Al4V substrates manufactured by E-PBF

Sample ID	Internal diameter (nm)	Length (μm)	Circularity
M1	65.24 ± 6.14	1.27 ± 0.07	0.97
M2	68.06 ± 5.51	1.09 ± 0.03	0.94
M3	128.46 ± 9.85	4.67 ± 0.14	0.95
M4	———	1.51 ± 0.14	—-
M5	———	0.37 ± 0.05	—-
M6	67.65 ± 9.96	1.26 ± 0.08	0.95
M7	———	1.22 ± 0.03	—-

have a layer on the top; this layer has been reported in previous articles [42, 49], and it is called the initiation layer, which is formed in the first stage of the anodization process. This layer is dissolved as the anodizing process progresses. The formation of nanotubes at 1000 s corroborates the information in Fig. 3, which states that stage 3 starts at about 500 s. From Fig. 2, organized nanotubes were formed at an anodization time of 2500 s; however, the initiation layer is seen in some parts of the nanotube top. On the other hand, at an anodization time of 5000 s, organized nanotubes were formed free of the initiation layer. Table 3 shows no difference between the internal diameter values of M6 and M1 (2500 and 5000 s); however, the nanotube length increases with the anodization time. Our findings are consistent with earlier experimental research [44, 50, 51] that have revealed the link between anodizing time and nanotube length.

Concerning the effect of anodizing voltage on the TiO_2 nanotube morphology and homogeneity, we evaluated two voltage values (30 and 60 V) which correspond to the M1 and M3 samples. Figures 2 and 4 and Table 3 show that the nanotube's internal diameter and length increase with the rise of the voltage. Our findings agree with earlier experimental reports on the link between nanotubes' internal diameter and length with the voltage. From Fig. 2, over the nanotubes produced at 60 V, there are rectangular and elongated particles linked to the nanotube walls. From the scientific literature [52, 53], those particles are called nanowires. According to Hsu et al. [52], the nanowires over the TiO_2 nanotubes are produced due to the fluoride ions attacking the nanotube near the mouth, which is the site where the nanotube wall is thinner, forming holes in the nanotube wall, those holes are disseminated, and finally, they expanded and becoming nanowires. The authors report that nanowires' presence over the nanotubes depends on the anodizing time and the voltage. From our results, the only difference between the M1 and M3 samples is the voltage value; thus, the potential of 60 V is the reason for the nanowires' presence in the M3 sample.

Typically, fluoride compounds vary from 0.20 to 1 in wt. % in the anodizing solution that is employed to produce TiO_2 nanotubes. Lower fluoride concentrations encourage the growth of the barrier layer rather than the nanotube structures. On the other hand, the oxide layer dissolves quickly at greater fluoride concentrations, which prevents the formation of nanotube structures. To produce clean and homogeneous nanotubes without compromising their properties, it is essential to ascertain the lowest concentration that can be used. Thus, we evaluated two NH_4F concentrations: 0.2 and 0.4 wt.%, corresponding to the samples M7 and M1, respectively. From Fig. 2, in the M7 sample, a porous nanostructure is seen; however, from Fig. 4, this porous structure

is thin and over the nanotubes. From the scientific literature [42, 54], this layer corresponds to an initiation layer. On the other hand, in M1 samples, the nanotubes are organized and free of the initiation layer; thus, the electrolyte with an NH_4F concentration of 0.4 wt.% is capable of dissolving this initiation layer. Table 3 shows no difference between the nanotube length values between the samples M7 and M1. From the literature [55, 56], the increase in fluoride concentrations produces a rise in the nanotube length. Our results disagree with the findings of these investigations.

TiO_2 nanotube formation by anodization depends heavily on the presence of water molecules in the electrolyte [44, 57]. The ionization of H_2O provides the oxygen to form TiO_2 in the first stage of the anodization process; furthermore, it generates the H^+ necessary to dissolve the TiO_2 to produce nanotubular structures [57]. A lack of water content in the electrolyte prevents the nanotube formation due to the lower H^+ concentration; on the other hand, an excess of water generates a higher chemical dissolution of TiO_2, causing the collapse of the TiO_2 nanotubes or, in some cases, a disorganized nanotube structure [56–58]. Thus, determining the lowest H_2O concentration that can be employed is crucial for producing clean and homogeneous nanotubes. Hence, we evaluated two H_2O concentrations: 4.5 and 9 vol%, corresponding to the samples M4 and M1, respectively. Figure 2 shows a porous nanostructure in the M4 sample; nevertheless, Fig. 4 shows that this porous structure is thin and covers the nanotubes; this thin layer has the morphology of an initiation layer. In contrast, the nanotubes in M1 samples are well organized and devoid of the initiation layer; thus, according to our results, it is necessary to use an H_2O concentration of 9 vol% to dissolve the initiation layer. From Table 3, the length diminished with the rise of water content. The reports found in the literature [56, 57] show that the increased water concentration enhances the electrolyte capacity of dissolving the TiO_2, producing shorter nanotubes. Our findings concur with those from these investigations.

However, qualitative and quantitative measurements of the nanotube order were possible; measuring ordering qualitatively using FFT pictures from SEM pictures may be feasible. Aguirre et al. [19] assessed the FFT pictures' shape acquired from SEM micrographs of TiO_2 nanotubes produced in aqueous electrolytes with carboxymethyl cellulose (CMC). The authors found that in less organized nanotube structures, the FFT form can adopt a variety of geometrical shapes, including rectangles and ellipses. Sometimes when the organization is zero, a fuzzy, ill-defined image is seen [59]. However, a more organized nanotube structure had an FFT picture with a circular shape. Figure 5 displays FFT images from SEM images of TiO_2 nanotubes obtained on Ti6Al4V substrates manufactured by E-PBF. From Fig. 5, all the FFT images have a circular shape; thus, making quantitative measurements of the nanotube ordering is necessary.

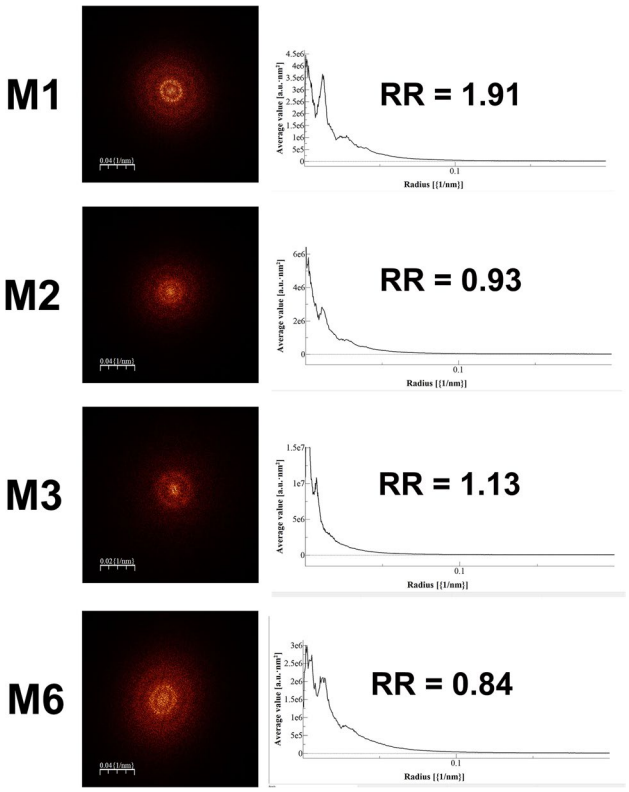

Fig. 5 FFT images and regularity ratios acquired from SEM images of TiO_2 nanotubes obtained on Ti6Al4V substrates manufactured by E-PBF

From Fig. 5, the FFT of M1 and M6 samples have concentric circles, indicating a long-range order in the TiO_2 nanotubes produced in these samples [59].

Based on the work of Stępniowski et al. [60], regularity ratio (RR) was calculated, which is based on FFT radial average. Its equation is as follows:

$$\mathrm{RR} = \frac{(I)(\sqrt{n})}{\left(W_{1/2}\right)\left(S^{\frac{3}{2}}\right)}$$

where S is the area, $W_{1/2}$ is the radial average's width at half its height, n is the number of nanotubes analyzed, and I is the radial average's intensity. A higher RR value indicates a better nanotube organization and homogeneity. The RR measurements in Fig. 5 could be related to the anodizing process parameters. Comparing the RR values of M1 and M2 samples, it is evident that the stirring affects the nanotube organization; according to our results, the nanotube organization increases in the absence of stirring. Concerning the voltage, the RR value of the M1 sample is higher than the M3 sample, indicating that the nanotube organization increases at lower voltages. However, the RR values of M2 and M3 could be affected by particles or incompletely dissolved oxide layers on the nanotube top. Regarding the

anodizing time effect on nanotube organization, the RR value of the M1 sample is higher than the M6 samples, indicating that although at 2500 s there are organized nanotubes, it is necessary longer anodization times to obtain highly ordered TiO_2 nanotubes.

The M1 sample has the highest RR value, which corresponds to 1.91; comparing this value to previous reports of TiO_2 is double of the highest value (0.97) obtained by Aguirre et al. [19], which used aqueous electrolytes with CMC and more than the double of the maximum value (0.75) obtained by Syauqi et al. [61] which used aqueous electrolytes with sodium alginate. To the best of our knowledge, there are no previous reports that use the methodology of Stępniowski et al. [60] in TiO_2 nanotubes obtained in organic electrolytes; however, the highest value of RR obtained in this experimental work is similar to the highest values obtained nanoporous anodic aluminum oxide in previous works [60, 62].

Comparing our results with the previous reports of TiO_2 nanotubes obtained in both Ti6Al4V substrates manufactured by additive manufacturing and forging, we consider that the stirring is a poorly studied critical anodization condition. In our case, combining the absence of stirring with the control of anodization time, voltage, and bath composition, we could obtain highly ordered TiO_2 nanotubes free of delamination, cracks, and coral-like structures.

Figure 6 shows the Raman spectra for the TiO_2 nanotubes obtained on Ti6Al4V substrates manufactured by E-PBF. All samples evaluated display similar spectra. The Raman spectra display wide peaks of about 150, 450, and 600 cm; other authors have described this spectrum's shape in earlier works [17, 18, 20, 63], which corresponds to amorphous TiO_2 nanotubes.

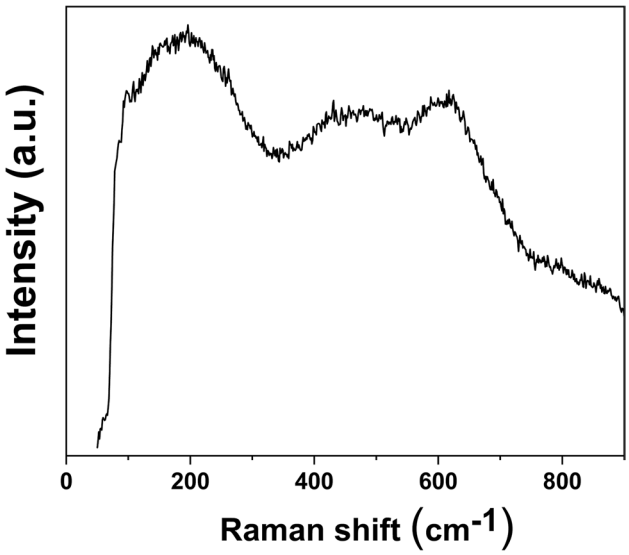

Fig. 6 Raman spectra of nanotubular coatings obtained on Ti6Al4V substrates manufactured by E-PBF

4 Conclusions

Highly ordered TiO_2 nanotubes were successfully produced on Ti6Al4V substrates manufactured by E-PBF. With careful control of the anodization parameter such as anodizing time, stirring, fluoride concentration, and water content is possible to obtain clean and highly ordered TiO_2 nanotubes avoiding the use of post-treatments such as ultrasonic cleaning. The nanotube ordering was affected by the voltage, stirring, and anodizing time. The internal diameter was altered only by the voltage; however, the nanotube length was affected by anodizing time, voltage, and water content.

Acknowledgements The authors are grateful to Instituto Tecnológico Metropolitano (Project PE21101), Universidad de Antioquia (2021-41090), Mid Sweden University, Centro de Investigación para el Desarrollo y la Innovación (CIDI) from the Universidad Pontificia Bolivariana (Rad: 636C-11/20-35), and Corporación Ruta N. The authors also thanks to the other institutions that are part of the G8+1 group: Corporación Universitaria Lasallista, Universidad CES, Universidad Eafit, Universidad EIA, Universidad de Medellín and Universidad Nacional de Colombia sede Medellín. R.A. and J.A.T. were supported by COLCIENCIAS (currently Minciencias) PhD grants.

Author contribution All authors contributed to the study conception and design. Material preparation, data collection, and analysis were performed by Robinson Aguirre Ocampo, Nicolás Bedoya, and Alejandro A. Zuleta Gil. The first draft of the manuscript was written by Robinson Aguirre Ocampo, and all authors commented on previous versions of the manuscript. All authors read and approved the final manuscript.

Funding Open Access funding provided by Colombia Consortium

Declarations

Competing interests The authors declare no competing interests.

References

1. Shahsavari M, Imani A, Schaller RF, Asselin E (2022) Corrosion evaluation of Ti–6Al–4V manufactured by electron beam melting

in Ringer's physiological solution: an in vitro study of the passive film. J Appl Electrochem 52:1003–1019. https://doi.org/10.1007/s10800-022-01683-0
2. Han X, Yang J, Li J, Wu J (2022) Constitutive modeling on the Ti-6Al-4V alloy during air cooling and application. Metals (Basel) 12(3):513. https://doi.org/10.3390/met12030513
3. Vaché N, Cadoret Y, Dod B, Monceau D (2021) Modeling the oxidation kinetics of titanium alloys: review, method and application to Ti-64 and Ti-6242s alloys. Corros Sci 178:109041. https://doi.org/10.1016/j.corsci.2020.109041
4. Dehnavi V, Henderson JD, Dharmendra C et al (2020) Corrosion behaviour of electron beam melted Ti6Al4V: effects of microstructural variation. J Electrochem Soc 167:131505. https://doi.org/10.1149/1945-7111/abb9d1
5. Titanium alloy market: global industry trends, share, size, growth, opportunity and forecast 2023–2028. imarcgroup. https://www.imarcgroup.com/titanium-alloy-market. Accessed 25 Dec 2022
6. Global Ti-6Al-4V Titanium alloy market 2022–2026. Infiniti Research Limited. https://www.reportlinker.com/p06360309/Global-Ti-6Al-4V-Titanium-Alloy-Market.html?utm_source=GNW. Accessed 25 Dec 2022
7. Li KM, Liu YJ, Liu XC, Wu X, Zhou SF, Zhang LC, Li W, Zhang WC (2022) Simultaneous strength-ductility enhancement in as-cast Ti6Al4V alloy by trace Ce. Mater Des 215:110491. https://doi.org/10.1016/j.matdes.2022.110491
8. Tshephe TS, Akinwamide SO, Olevsky E, Olubambi PA (2022) Additive manufacturing of titanium-based alloys- a review of methods, properties, challenges, and prospects. Heliyon 8:e09041. https://doi.org/10.1016/j.heliyon.2022.e09041
9. Sopha H, Kashimbetova A, Hromadko L et al (2021) Anodic TiO2 nanotubes on 3D-printed titanium meshes for photocatalytic applications. Nano Lett 21:8701–8706. https://doi.org/10.1021/acs.nanolett.1c02815
10. Dutta B, Froes FH (2016) Additive manufacturing of titanium alloys: state of the art, challenges and opportunities
11. Zhang T, Liu C-T (2022) Design of titanium alloys by additive manufacturing: a critical review. Adv Powder Mater 1:100014. https://doi.org/10.1016/j.apmate.2021.11.001
12. Montelione A, Ghods S, Schur R et al (2020) Powder reuse in electron beam melting additive manufacturing of Ti6Al4V: particle microstructure, oxygen content and mechanical properties. Addit Manuf 35:101216. https://doi.org/10.1016/j.addma.2020.101216
13. Karlsson J, Norell M, Ackelid U et al (2015) Surface oxidation behavior of Ti-6Al-4V manufactured by Electron Beam Melting (EBM®). J Manuf Process 17:120–126. https://doi.org/10.1016/j.jmapro.2014.08.005
14. Tamayo JA, Riascos M, Vargas CA, Baena LM (2021) Additive manufacturing of Ti6Al4V alloy via electron beam melting for the development of implants for the biomedical industry. Heliyon 7(5):e06892. https://doi.org/10.1016/j.heliyon.2021.e06892
15. Bertsch KM, Voisin T, Forien JB et al (2022) Critical differences between electron beam melted and selective laser melted Ti-6Al-4 V. Mater Des 216:110533. https://doi.org/10.1016/j.matdes.2022.110533
16. Silvestri AT, Foglia S, Borrelli R et al (2020) Electron beam melting of Ti6Al4V: role of the process parameters under the same energy density. J Manuf Process 60:162–179. https://doi.org/10.1016/j.jmapro.2020.10.065
17. Aguirre R, Echeverry-Rendón M, Quintero D, Castaño JG, Harmsen MC, Robledo S, Echeverría EF (2018) Formation of nanotubular TiO2 structures with varied surface characteristics for biomaterial applications. J Biomed Mater Res - Part A 106(5). https://doi.org/10.1002/jbm.a.36331
18. Aguirre Ocampo R, Echeverría EF (2018) Effects of fluoride source on the characteristics of titanium dioxide nanotubes. Appl Surf Sci 445:308–319. https://doi.org/10.1016/j.apsusc.2018.03.139
19. Aguirre Ocampo R, Echeverría Echeverría F (2019) Effect of the anodization parameters on TiO2 nanotubes characteristics produced in aqueous electrolytes with CMC. Appl Surf Sci 469:994–1006. https://doi.org/10.1016/j.apsusc.2018.11.097
20. Aguirre Ocampo R, Echeverría Echeverría F (2022) TiO2 nanotubes produced on thin titanium wires using aqueous electrolytes. Mater Manuf Process 00:1–7. https://doi.org/10.1080/10426914.2022.2116037
21. Aguirre Ocampo R, Echeverría Echeverría F (2021) TiO2 nanotubes produced on curved titanium surfaces using aqueous electrolytes with carboxymethyl cellulose. Phys E Low-dimensional Syst Nanostruct 125:114391. https://doi.org/10.1016/j.physe.2020.114391
22. Aguirre Ocampo R, Echeverry-Rendón M, DeAlba-Montero I et al (2021) Effect of surface characteristics on the antibacterial properties of TiO2 nanotubes produced in aqueous electrolytes with carboxymethyl cellulose. J Biomed Mater Res Part A 109:104–121. https://doi.org/10.1002/jbm.a.37010
23. Aguirre Ocampo R, Echeverría Echeverría F (2021) Antibacterial and biological behavior of TiO2 nanotubes produced by anodizing technique. Crit Rev Biomed Eng 49:51–65. https://doi.org/10.1615/CritRevBiomedEng.2021037758
24. Galstyan V, Macak JM, Djenizian T (2022) Anodic TiO2 nanotubes: a promising material for energy conversion and storage. Appl Mater Today 29:101613. https://doi.org/10.1016/j.apmt.2022.101613
25. Wang Q, Huang JY, Li HQ et al (2017) Recent advances on smart TiO2 nanotube platforms for sustainable drug delivery applications. Int J Nanomedicine 12:151–165. https://doi.org/10.2147/IJN.S117498
26. Asgari V, Noormohammadi M, Ramazani A, Kashi MA (2017) A facile method to form highly-ordered TiO2nanotubes at a stable growth rate of 1000 nm min-1under 60 v using an organic electrolyte for improved photovoltaic properties. J Phys D Appl Phys 50(37). https://doi.org/10.1088/1361-6463/aa812a
27. Mohammadi T, Sharifi S, Ghayeb Y, et al (2022) Photoelectrochemical water splitting and H2 generation enhancement using an effective surface modification of W-doped TiO2 nanotubes (WT) with co-deposition of transition metal ions. Sustain 14(20):13251. https://doi.org/10.3390/su142013251
28. Di Yao D, Field MR, O'Mullane AP et al (2013) Electrochromic properties of TiO2 nanotubes coated with electrodeposited MoO3. Nanoscale 5:10353–10359. https://doi.org/10.1039/C3NR03666A
29. Ribeiro B, Offoiach R, Rossetti S, Salatin E, Lekka M, Fedrizzi L (2022) On growth and morphology of TiO2 nanotubes on CP-Ti by anodic oxidation in ethylene glycol electrolyte: influence of electrolyte aging and anodization parameters. Materials 15(9):3338. https://doi.org/10.3390/ma15093338
30. Aguirre Ocampo R, Echeverry-Rendón M, Robledo S, Echeverría Echeverría F (2022) Effect of TiO2 nanotubes size, heat treatment, and UV irradiation on osteoblast behavior. Mater Chem Phys 275:125137. https://doi.org/10.1016/j.matchemphys.2021.125137
31 Macak JM, Tsuchiya H, Ghicov A et al (2007) TiO2 nanotubes: self-organized electrochemical formation, properties and applications. Curr Opin Solid State Mater Sci 11:3–18. https://doi.org/10.1016/j.cossms.2007.08.004
32. Horcas I, Fernández R, Gomez-Rodriguez JM, Colchero J, Gómez-Herrero J, Baro AM (2007) WSXM: a software for scanning probe microscopy and a tool for nanotechnology. Rev Sci Instrum 78(1):013705. https://doi.org/10.1063/1.2432410

33. Tan X, Kok Y, Tan YJ et al (2015) Graded microstructure and mechanical properties of additive manufactured Ti-6Al-4V via electron beam melting. Acta Mater 97:1–16. https://doi.org/10.1016/j.actamat.2015.06.036
34. Sharma H, Parfitt D, Syed AK et al (2019) A critical evaluation of the microstructural gradient along the build direction in electron beam melted Ti-6Al-4V alloy. Mater Sci Eng A 744:182–194. https://doi.org/10.1016/j.msea.2018.12.016
35. Jamshidinia M, Atabaki MM, Zahiri M et al (2015) Microstructural modification of Ti-6Al-4V by using an in-situ printed heat sink in Electron Beam Melting® (EBM). J Mater Process Technol 226:264–271. https://doi.org/10.1016/j.jmatprotec.2015.07.006
36. Jordanovová V, Losertová M, Štencek M et al (2020) Microstructure and properties of nanostructured coating on Ti6Al4V. Materials (Basel) 13:1–11. https://doi.org/10.3390/ma13030708
37. Fraoucene H, Sugiawati VA, Hatem D et al (2019) Optical and electrochemical properties of self-organized TiO2 nanotube arrays from anodized Ti-6Al-4V alloy. Front Chem 7:1–9. https://doi.org/10.3389/fchem.2019.00066
38. Decha-umphai D, Chunate H, Phetrattanarangsi T et al (2021) Effects of post-processing on microstructure and adhesion strength of TiO2 nanotubes on 3D-printed Ti-6Al-4V alloy. Surf Coatings Technol 421:127431. https://doi.org/10.1016/j.surfcoat.2021.127431
39. Apolinário A, Sousa CT, Ventura J et al (2014) The role of the Ti surface roughness in the self-ordering of TiO2 nanotubes: a detailed study of the growth mechanism. J Mater Chem A 2:9067. https://doi.org/10.1039/c4ta00871e
40. Apolinário A, Quitério P, Sousa CT et al (2015) Modeling the growth kinetics of anodic TiO2 nanotubes. J Phys Chem Lett 6:845–851. https://doi.org/10.1021/jz502380b
41. Quitério P, Apolinário A, Sousa CT et al (2015) The cyclic nature of porosity in anodic TiO2 nanotube arrays. J Mater Chem A 3:3692–3698. https://doi.org/10.1039/C4TA04607B
42. Montakhab E, Rashchi F, Sheibani S (2020) Modification and photocatalytic activity of open channel TiO2 nanotubes array synthesized by anodization process. Appl Surf Sci 534:147581. https://doi.org/10.1016/j.apsusc.2020.147581
43. Liu H, Tao L, Shen W (2011) Controllable current oscillation and pore morphology evolution in the anodic growth of TiO2 nanotubes. Nanotechnology 22:155603. https://doi.org/10.1088/0957-4484/22/15/155603
44. Puga ML, Venturini J, ten Caten CS, Bergmann CP (2022) Influencing parameters in the electrochemical anodization of TiO2 nanotubes: systematic review and meta-analysis. Ceram Int 48:19513–19526. https://doi.org/10.1016/j.ceramint.2022.04.059
45. Li H, Ding M, Jin J et al (2018) Effect of electrolyte pretreatment on the formation of TiO2 nanotubes: an ignored yet non-negligible factor. ChemElectroChem 5:1006–1012. https://doi.org/10.1002/celc.201701231
46. Hwang HY, Prabu AA, Kim DY, Kim KJ (2011) Influence of the organic electrolyte and anodization conditions on the preparation of well-aligned TiO2 nanotube arrays in dye-sensitized solar cells. Sol Energy 85:1551–1559. https://doi.org/10.1016/j.solener.2011.04.017
47. Liu R, Yang WD, Qiang LS, Wu JF (2011) Fabrication of TiO2 nanotube arrays by electrochemical anodization in an NH4F/H3PO4 electrolyte. Thin Solid Films 519:6459–6466. https://doi.org/10.1016/j.tsf.2011.04.231
48. Xu H, Zhang Q, Zheng C et al (2011) Application of ultrasonic wave to clean the surface of the TiO2 nanotubes prepared by the electrochemical anodization. Appl Surf Sci 257:8478–8480. https://doi.org/10.1016/j.apsusc.2011.04.135
49. Albu SP, Schmuki P (2010) Highly defined and ordered top-openings in TiO2 nanotube arrays. Phys Status Solidi - Rapid Res Lett 4:151–153. https://doi.org/10.1002/pssr.201004159
50. Regonini D, Clemens FJ (2015) Anodized TiO2nanotubes: effect of anodizing time on film length, morphology and photoelectrochemical properties. Mater Lett 142:97–101. https://doi.org/10.1016/j.matlet.2014.11.145
51. Li DG, Chen DR, Wang JD, Liang P (2016) Effect of acid solution, fluoride ions, anodic potential and time on the microstructure and electronic properties of self-ordered TiO2nanotube arrays. Electrochim Acta 207:152–163. https://doi.org/10.1016/j.electacta.2016.04.002
52. Hsu M-Y, Hsu H-L, Leu J (2012) TiO 2 nanowires on anodic TiO 2 nanotube arrays (TNWs/TNAs): formation mechanism and photocatalytic performance. J Electrochem Soc 159:H722–H727. https://doi.org/10.1149/2.063208jes
53. Uyen NN, Tuyen LTC, Hieu LT, Nguyen TTT, Thao HP, Do TCMV, Nguyen KT, Hang NTN, Jian SR, Tu LA et al (2022) TiO2 nanowires on TiO2 Nanotubes arrays (TNWs/TNAs) decorated with Au nanoparticles and Au nanorods for efficient photoelectrochemical water splitting and photocatalytic degradation of methylene blue. Coatings 12(12):1957. https://doi.org/10.3390/coatings12121957
54. Mazare A (2022) Comment on "old is gold: electrolyte aging influences the topography, chemistry, and bioactivity of anodized TiO2 nanopores." ACS Appl Mater Interfaces 14:14837–14841. https://doi.org/10.1021/acsami.1c18860
55. Wang X, Li Y, Song H et al (2016) Fluoride concentration controlled TiO2 nanotubes: the interplay of microstructure and photocatalytic performance. RSC Adv 6:18333–18339. https://doi.org/10.1039/C5RA24732B
56. Acevedo-Peña P, Lartundo-Rojas L, González I (2013) Effect of water and fluoride content on morphology and barrier layer properties of TiO2 nanotubes grown in ethylene glycol-based electrolytes. J Solid State Electrochem 17:2939–2947. https://doi.org/10.1007/s10008-013-2212-2
57. Sun Y, Zhao Q, Wang G, Yan K (2017) Influence of water content on the formation of TiO2 nanotubes and photoelectrochemical hydrogen generation. J Alloys Compd 711:514–520. https://doi.org/10.1016/j.jallcom.2017.03.007
58. Indira K, Mudali UK, Nishimura T, Rajendran N (2015) A review on TiO2 nanotubes: influence of anodization parameters, formation mechanism, properties, corrosion behavior, and biomedical applications. J Bio- Tribo-Corrosion 1:28. https://doi.org/10.1007/s40735-015-0024-x
59. Farsinezhad S, Dalrymple AN, Shankar K (2014) Toward single-step anodic fabrication of monodisperse TiO2 nanotube arrays on non-native substrates. Phys Status Solidi Appl Mater Sci 211:1113–1121. https://doi.org/10.1002/pssa.201330649
60. Stępniowski WJ, Michalska-Domańska M, Norek M, Czujko T (2014) Fast Fourier transform based arrangement analysis of poorly organized alumina nanopores formed via self-organized anodization in chromic acid. Mater Lett 117:69–73. https://doi.org/10.1016/j.matlet.2013.11.099
61. Syauqi MI, Prasetia P, Gunlazuardi J (2023) The influence of sodium alginate in water-based electrolyte on the morphology of TiO 2 nanotube prepared by anodization method. Mater Chem Phys 296:127234. https://doi.org/10.1016/j.matchemphys.2022.127234
62. Stepniowski WJ, Michalska-Domańska M, Norek M et al (2014) Anodization of cold deformed technical purity aluminum (AA1050) in oxalic acid. Surf Coatings Technol 258:268–274. https://doi.org/10.1016/j.surfcoat.2014.09.013
63. Hardcastle F (2011) Raman spectroscopy of titania (TiO2) nanotubular water-splitting catalysts. J Ark Acad Sci 65:43–48. https://doi.org/10.54119/jaas.2011.6504